

# First-principles predictions of band alignment in strained Si/Si<sub>1-x</sub>Ge<sub>x</sub> and Ge/Si<sub>1-x</sub>Ge<sub>x</sub> heterostructures

Nathaniel M. Vegh,<sup>1,2,a)</sup> Pericles Philippopoulos,<sup>1</sup> Raphaël J. Prentki,<sup>1</sup> Wanting Zhang,<sup>1</sup> Yu Zhu,<sup>1</sup> Félix Beaudoin,<sup>1</sup> and Hong Guo<sup>2</sup>

<sup>1)</sup>*Nanoacademic Technologies Inc., Montréal, Suite 802, 666 rue Sherbrooke Ouest, Montréal, Québec, Canada H3A 1E7*

<sup>2)</sup>*Department of Physics, McGill University, Montréal, QC H3A 0G4, Canada*

(Dated: March 13, 2026)

Accurate band offsets are essential for predictive continuum modeling of nanostructures such as quantum wells and quantum dots formed in strained Si/Si<sub>1-x</sub>Ge<sub>x</sub> and Ge/Si<sub>1-x</sub>Ge<sub>x</sub> heterostructures. Experimental offset data for these systems remain sparse away from endpoint compositions, which makes composition-dependent design difficult. We use atomistic, first-principles density functional theory to compute valence- and conduction-band offsets across the full range  $0 \leq x \leq 1$ . Random alloying is treated with special quasirandom structures, interface lineup terms are extracted from macroscopically averaged local Kohn–Sham potentials in thick periodic superlattices, valence-band spin–orbit coupling is included through species-resolved Mulliken weights, and conduction-band edges are refined using the screened hybrid Heyd–Scuseria–Ernzerhof functional. The resulting offsets show pronounced composition nonlinearity beyond the linear models explored in previous works, agree with experimental benchmarks, and reproduce the high-Ge slope change in the relaxed-alloy band gap. Analytic fitting expressions are provided for direct use in simulations, facilitating practical design of modern quantum technology devices.

Strained Si/Si<sub>1-x</sub>Ge<sub>x</sub> and Ge/Si<sub>1-x</sub>Ge<sub>x</sub> heterostructures are central to modern electronic and quantum devices, including high-mobility transistors, modulation-doped quantum wells, and electron and hole quantum dots.<sup>1–6</sup> In these platforms, valence- and conduction-band offsets enter directly as material parameters in continuum electrostatics workflows used to predict confinement potentials, tunnel barriers, and qubit performance.<sup>3,7,8</sup> Reliable offsets across composition are therefore required to separate genuine device-physics from uncertainty in material inputs.

A first-principles description of band alignment decomposes the offset into (i) a bulk band-edge term, defined relative to a reference potential in each material, and (ii) an interface-lineup term, which captures charge rearrangement and the resulting interface dipole.<sup>9–12</sup> Compared with Anderson’s electron-affinity rule,<sup>13</sup> which aligns materials using vacuum-referenced electron affinities, this decomposition uses an explicit interface electrostatic lineup and avoids the ambiguities of vacuum-level alignment.<sup>9,12</sup> For isovalent Si/Ge-derived interfaces, prior first-principles analyses indicate that interface dipoles from interdiffusion or atom exchange across the interface are typically small, while strain-driven band-edge shifts and splittings remain central to quantitative offsets.<sup>9–11</sup> In strained SiGe systems, the lineup problem is coupled to strain-induced band-edge shifts and splittings,<sup>11,14,15</sup> while random-alloy disorder introduces finite-size and configuration-sampling effects that must be quantified.

Experimentally, band-offset extraction in Si/Ge/SiGe systems remains challenging and is often limited to specific structures or compositions. This is particularly relevant because the most common spin-qubit regimes already cluster around strained-Si wells on Si-rich SiGe barriers with  $x \approx 0.25$ – $0.33$  and strained-Ge wells on Ge-rich SiGe barriers with

$x \approx 0.6$ – $0.9$ , often near  $x \approx 0.8$ .<sup>1,4,6</sup> Representative benchmarks include core-level photoemission on pseudomorphic Si/Ge interfaces,<sup>16</sup> Ge/Si<sub>1-x</sub>Ge<sub>x</sub> photoreflectance at a few Ge-rich barrier compositions,<sup>17</sup> and selected Si/Si<sub>1-x</sub>Ge<sub>x</sub> measurements compiled by Van de Walle.<sup>11</sup> These studies provide key anchor points, but they do not by themselves deliver a dense, internally consistent dataset for both strained Si/Si<sub>1-x</sub>Ge<sub>x</sub> and Ge/Si<sub>1-x</sub>Ge<sub>x</sub> across  $0 \leq x \leq 1$ .

On the modeling side, parameter compilations and analytic models are invaluable for simulation practice,<sup>1–3,11,18</sup> yet they are assembled from heterogeneous experiments and theoretical assumptions and are not always internally consistent across strain states, compositions, and interface structures. This gap motivates a single, internally consistent first-principles dataset across the full composition range. Here we apply one procedure throughout: explicit interface-lineup extraction in thick periodic superlattices, special quasirandom structure (SQS) treatment of random alloys, a Mulliken-weight spin–orbit-coupling (SOC) correction of the valence edge, and hybrid-functional refinement of conduction edges.

All calculations are performed using the real-space density-functional theory (DFT) package RESCU,<sup>19,20</sup> and employ the Perdew–Burke–Ernzerhof (PBE) generalized-gradient approximation (GGA) for the exchange–correlation (XC) energy.<sup>21</sup> To correct the semilocal band-gap error in the conduction offsets, we later refine the conduction-edge terms with the Heyd–Scuseria–Ernzerhof (HSE) hybrid functional while retaining the PBE lineup workflow. The wavefunctions are represented in a linear combination of atomic orbitals (LCAO) basis.<sup>19</sup> Bulk band-edge calculations are performed in 64-atom supercells (Si<sub>1-x</sub>Ge<sub>x</sub> SQS built from a  $2 \times 2 \times 2$  replication of the conventional cubic cell)<sup>22</sup> using a  $3 \times 3 \times 3$  Monkhorst–Pack  $k$ -point grid.<sup>23</sup> For lineup extraction, we use thick periodic heterostructure superlattices (512 atoms) sampled with a  $3 \times 3 \times 1$  Monkhorst–Pack  $k$ -point grid. All bulk and heterostructure calculations use three-dimensional periodic boundary conditions defined by the supercell lattice

<sup>a)</sup>Electronic mail: nathaniel.vegh@mail.mcgill.ca

vectors and sampled over the corresponding Brillouin zone. Structural relaxations are performed at fixed in-plane lattice constants set by the relaxed alloy buffer (epitaxial constraint), while internal coordinates and the out-of-plane lattice parameter are relaxed to the numerical force/stress convergence thresholds. In strained bulk reference cells,  $E_v$  and  $E_c$  denote the valence-band maximum (VBM) and conduction-band minimum (CBM) energies and are taken as the highest occupied and lowest unoccupied Kohn–Sham eigenvalues over the sampled Brillouin-zone mesh.<sup>9,10,12</sup> Operationally,  $E_v$  ( $E_c$ ) is the maximum (minimum) eigenvalue with occupation threshold  $n_{\text{occ}} > 10^{-3}$  ( $< 10^{-3}$ ), and bulk band edges are measured relative to the cell-averaged local potential  $\langle v_{\text{dh}} + v_{\text{na}} + v_{\text{xc}} \rangle$ , where  $v_{\text{dh}}$  is the Hartree potential generated by the self-consistent charge redistribution,  $v_{\text{na}}$  is the neutral-atom potential used to assemble the atomic lattice, and  $v_{\text{xc}}$  is the exchange–correlation term.<sup>12,19</sup> Additional numerical details and convergence checks are provided in the Supplementary Material.

We consider strained Si and strained Ge on a relaxed  $\text{Si}_{1-x}\text{Ge}_x$  buffer at composition  $x$ , each biaxially constrained in plane to the buffer lattice constant. The buffer lattice constant  $a_{\parallel} = a_{\text{SiGe}}(x)$  is obtained by equation-of-state (EOS) total-energy minimization of isotropically scaled  $\text{Si}_{1-x}\text{Ge}_x$  SQS cells. Figure 1 summarizes the resulting lattice constants. For the random alloy, we construct SQS supercells designed to reproduce the pair correlations of a random SiGe alloy within a finite supercell.<sup>22</sup> For the primary interface-offset dataset reported in Supplementary Table S1, one SQS superlattice is used at each composition. For Fig. 2, three SQS configurations are averaged per composition. Additional repeated-SQS tests for both bulk alloys and interface superlattices were used to estimate configuration-induced fluctuations. The relaxed-alloy HSE gap shows a representative three-SQS full spread of about 50 meV, while the lineup term varies at about the 10 meV level across repeated tests; these values set the representative uncertainty model used for the offset error bars.

With the strain state and bulk reference quantities defined, we adopt the potential-lineup decomposition introduced by Van de Walle and Martin.<sup>9–12</sup> For a heterojunction between materials  $A$  and  $B$ , the valence-band offset (VBO) is

$$\Delta E_v = [E_v^B - \bar{V}^B] - [E_v^A - \bar{V}^A] + [\bar{V}^B - \bar{V}^A]_{\text{IF}} + \Delta E_{v,\text{SOC}}^{B/A}, \quad (1)$$

and similarly for the conduction-band offset (CBO),

$$\Delta E_c = [E_c^B - \bar{V}^B] - [E_c^A - \bar{V}^A] + [\bar{V}^B - \bar{V}^A]_{\text{IF}} + \Delta E_c^{\text{SOC}}. \quad (2)$$

To make the terms in Eqs. (1) and (2) explicit, we define the bulk macroscopic-averaged potential and lineup terms as follows. For each bulk reference cell  $X \in \{A, B\}$ , the bulk macroscopic-averaged potential is

$$\bar{V}^X = \frac{1}{\Omega_X} \int_{\Omega_X} (v_{\text{dh}} + v_{\text{na}} + v_{\text{xc}}) d^3r, \quad (3)$$

where  $\Omega_X$  is the bulk-cell volume. Using the same local-potential reference in both bulk and superlattice calculations

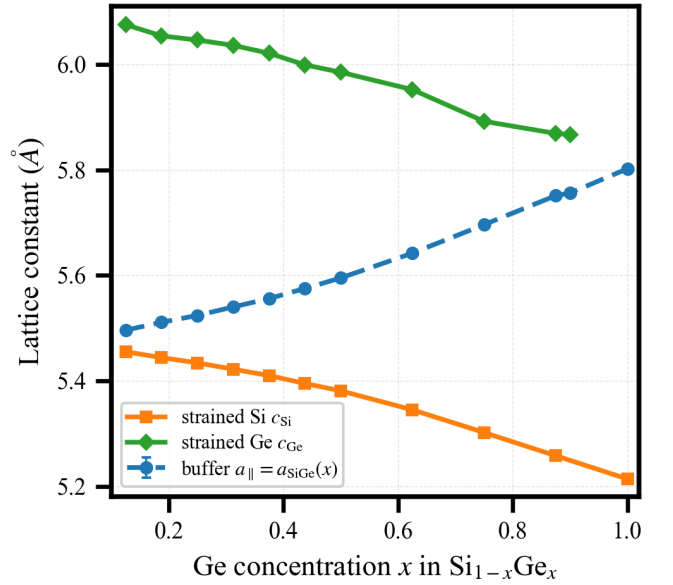


FIG. 1. Epitaxially constrained lattice constants used in this work. The relaxed-alloy buffer lattice constant  $a_{\parallel} = a_{\text{SiGe}}(x)$  is compared with the relaxed out-of-plane lattice constants  $c_{\text{Si}}$  and  $c_{\text{Ge}}$ . Error bars on  $a_{\parallel}$  show a representative  $\pm 0.001$  Å uncertainty from EOS-fitted SQS minima. The strained-Ge series is shown up to  $x = 0.9$ ;  $x = 1$  is the Ge/Ge homoepitaxial limit.

ensures strict internal consistency across the workflow. The interface lineup term is

$$\Delta V_{\text{IF}} \equiv [\bar{V}^B - \bar{V}^A]_{\text{IF}}, \quad (4)$$

where the subscript IF denotes the interface contribution extracted from an explicit periodic  $A/B$  superlattice and corresponds to the macroscopic potential step associated with the interface dipole.<sup>9,10</sup> In this work we apply SOC corrections only to the valence term and neglect an explicit  $\Delta E_c^{\text{SOC}}$ , consistent with prior SiGe band-offset treatments in which SOC is needed to determine the valence-band maximum accurately, while conduction offsets are obtained from the relevant  $X$ - and  $L$ -valley positions and band-gap differences.<sup>9,11</sup>

The lineup in Eq. (4) is extracted by computing the self-consistent local Kohn–Sham potential in a periodic heterostructure superlattice, planar-averaging along the growth direction  $z$ , and smoothing to remove atomic-scale oscillations.<sup>9,24</sup> All superlattices are oriented along the cubic [001] growth direction and constructed as coherent (001) Si/SiGe heterostructures with a  $2 \times 2$  in-plane repeat. A representative lineup cell contains 8 conventional cells of strained Si and 8 conventional cells of  $\text{Si}_{1-x}\text{Ge}_x$  (SQS) along  $z$  (256 atoms per side, 512 atoms total), yielding two interfaces per periodic supercell. The lineup is taken as the difference between plateau values in bulk-like regions sufficiently far from the interfaces. We emphasize that no vacuum region is used: the periodic superlattice contains only coherent  $A/B$  interfaces and avoids surface dipoles and termination sensitivity inherent to vacuum-level alignment. Here, plateau selection refers to choosing the bulk-like averaging windows on each side of the interface from which the potential step is measured. In prac-

tice, we planar-average the local potential along  $z$ , smooth it with a periodic error-function kernel of width 2.0 Å applied twice, and evaluate the plateau values from fixed bulk-like windows within each slab, away from the interfacial oscillations. Thickness convergence was checked by varying the number of conventional cells per side ( $N = 2, 4, 6, 8, 10, 12$ ); the extracted  $\Delta V_{\text{IF}}$  converges by  $N = 8$  within a typical tolerance of about 0.02 eV for representative compositions.

We apply a valence-band SOC correction based on species-resolved Mulliken populations:<sup>25</sup>

$$\Delta E_v^{\text{SOC}}(\text{SiGe}) \approx \sum_{\alpha \in \{\text{Si, Ge}\}} w_{\alpha} \Delta_{\alpha}, \quad (5)$$

In our LCAO representation,  $w_{\alpha}$  is computed from the VBM eigenvector as the normalized sum of Mulliken populations on basis functions centered on species  $\alpha$ ; physically, it is the fraction of VBM charge localized on that species. The species-resolved SOC shifts  $\Delta_{\alpha}$  are taken from tabulated elemental spin-orbit splittings from empirical-pseudopotential parameter compilations,<sup>14</sup> with  $\Delta_{\text{so}}^{\text{Si}} = 0.044$  eV and  $\Delta_{\text{so}}^{\text{Ge}} = 0.296$  eV. For valence states of predominantly  $p$  character, the upper ( $j = 3/2$ -derived) branch lies  $\Delta_{\text{so}}/3$  above the unsplit  $p$ -state center, so we use  $\Delta_{\alpha} \approx \Delta_{\text{so}}^{\alpha}/3$  in Eq. (5). The SOC contribution entering Eq. (1) is then

$$\Delta E_{v,\text{SOC}}^{B/A} = \Delta E_v^{\text{SOC}}(B) - \Delta E_v^{\text{SOC}}(A). \quad (6)$$

This approximation is physically motivated because the SOC operator is short-ranged around nuclei and the VBM in group-IV semiconductors is predominantly  $p$ -like. This construction separates the composition-dependent orbital character encoded in  $w_{\alpha}$  from the species-resolved SOC strength  $\Delta_{\alpha}$ , enabling an efficient correction without modifying the self-consistent charge density.

Semilocal DFT typically underestimates semiconductor band gaps, which can systematically bias conduction-band edges and therefore conduction-band offsets.<sup>12,26,27</sup> Screened hybrid functionals such as Heyd–Scuseria–Ernzerhof (HSE) reduce this error by replacing part of short-range semilocal exchange with exact exchange.<sup>26,27</sup> We therefore refine bulk conduction edges using HSE at selected strained Si and  $\text{Si}_{1-x}\text{Ge}_x$  compositions chosen to span the composition range and sample the high- $x$  regime, and combine these edges with the PBE interface-lineup term  $\Delta V_{\text{IF}}$  from thick superlattice simulations. We do not rerun the full 512-atom disordered superlattice simulations with HSE; this approximation is motivated by prior lineup analyses showing that lineup terms are primarily electrostatic (set by the self-consistent density and interface dipole), while absolute band-edge energies are more functional-sensitive.<sup>9,10,12</sup>

Figure 2 shows the HSE band gap of relaxed  $\text{Si}_{1-x}\text{Ge}_x$  across composition. A clear change in slope is observed at high Ge content, consistent with the known crossover in the character of the lowest conduction minimum in Ge-rich alloys.<sup>1,2</sup> Capturing this high- $x$  slope change provides an internal check that the bulk workflow and alloy structural modeling reproduce a key signature of the SiGe system relevant for conduction band alignment.

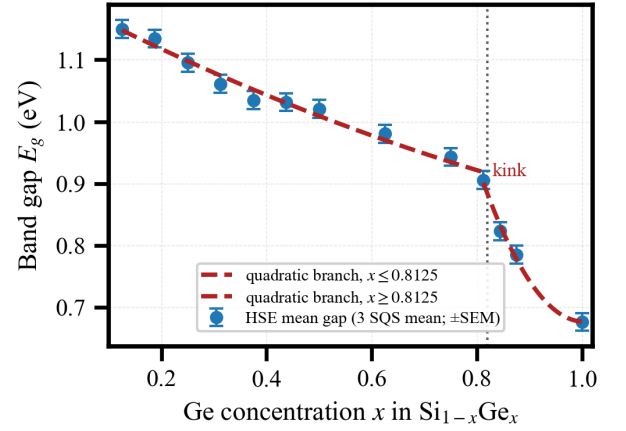


FIG. 2. HSE band gap of relaxed  $\text{Si}_{1-x}\text{Ge}_x$  across composition. Points show three-SQS means with representative standard-error bars derived from a characteristic full spread of about 50 meV. Dashed guides are overlapping quadratic fits with a crossover near  $x \approx 0.82$ .

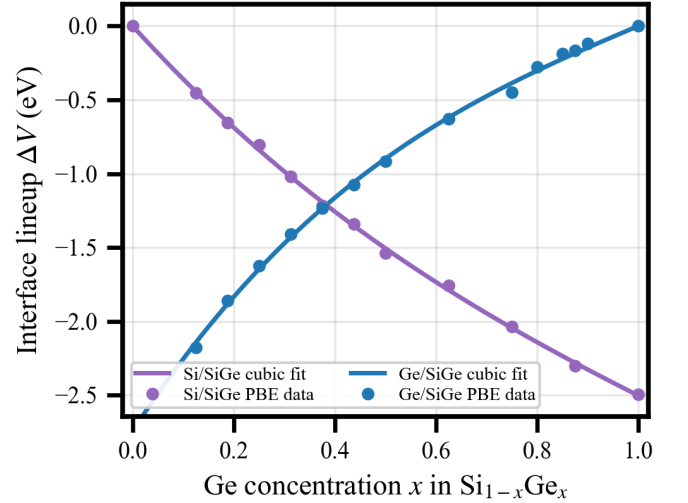


FIG. 3. Interface lineup  $\Delta V_{\text{IF}}$  as a function of Ge concentration  $x$  in  $\text{Si}_{1-x}\text{Ge}_x$  for strained Si/ $\text{Si}_{1-x}\text{Ge}_x$  and strained Ge/ $\text{Si}_{1-x}\text{Ge}_x$ , extracted from macroscopically averaged local Kohn–Sham potentials in thick periodic superlattices. The curves are constrained cubic fits satisfying  $\Delta V_{\text{IF}}(0) = 0$  for Si/Si and  $\Delta V_{\text{IF}}(1) = 0$  for Ge/Ge.

For strained Si on  $\text{Si}_{1-x}\text{Ge}_x$ , the hybrid functional mitigates semilocal gap error that can otherwise bias conduction-band offsets through the bulk band-edge term.

Figure 3 summarizes the lineup term  $\Delta V_{\text{IF}}$  across composition for both Si/ $\text{Si}_{1-x}\text{Ge}_x$  and Ge/ $\text{Si}_{1-x}\text{Ge}_x$  interfaces. At compositions with repeated alloy realizations, we average over independent SQS superlattices to suppress configuration noise. For practical use in device simulation, the interface lineup is represented by the following constrained cubic fits:

$$\begin{aligned} \Delta V_{\text{IF}}^{\text{Si/SiGe}}(x) &= -0.4878x^3 + 1.7497x^2 - 3.7635x, \\ \Delta V_{\text{IF}}^{\text{Ge/SiGe}}(x) &= 1.1837(x-1)^3 - 0.1159(x-1)^2 \\ &\quad + 1.4412(x-1). \end{aligned} \quad (7)$$

In Eq. (7),  $x$  is dimensionless and all coefficients are in eV. Combining the bulk band-edge terms with the fitted lineup expressions yields the full band offsets summarized in Fig. 4.

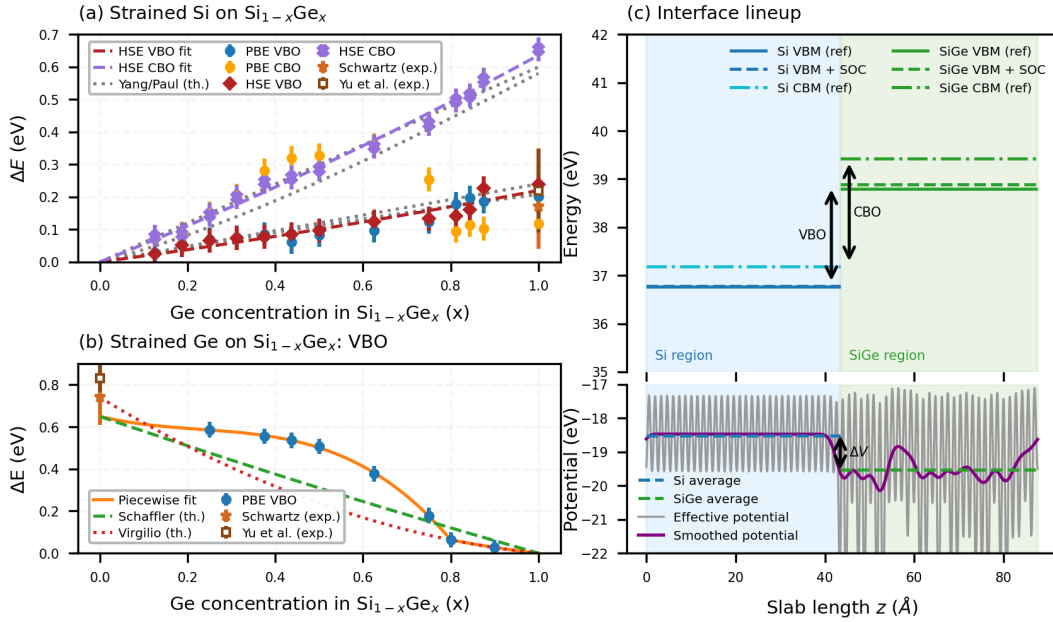


FIG. 4. Band-offset summary. (a) Strained-Si/ $\text{Si}_{1-x}\text{Ge}_x$  valence- and conduction-band offsets versus Ge concentration, with HSE fit guides. (b) Strained-Ge/ $\text{Si}_{1-x}\text{Ge}_x$  valence-band offset versus  $x$ , with theory curves and directly comparable endpoint photoemission data.<sup>1,16,18,28</sup> (a,b) Computed-point error bars combine two representative band-edge uncertainties inferred from the three-SQS gap spread with a 10 meV lineup term, added in quadrature; experimental bars are taken from the cited measurements. (c) Representative lineup extraction used to obtain  $\Delta V_{\text{IF}}$ .

For strained Si on relaxed  $\text{Si}_{1-x}\text{Ge}_x$ , HSE-refined conduction edges avoid severe semilocal-gap underestimation at large tensile strain and yield trends consistent with electron confinement in strained Si quantum wells on SiGe buffers.<sup>1-3</sup> For use in continuum device solvers such as QTCAD,<sup>29</sup> the HSE-refined strained-Si offsets are

$$\begin{aligned} \Delta E_v^{\text{HSE}}(x) &= 0.03848x^2 + 0.18158x, \\ \Delta E_c^{\text{HSE}}(x) &= 0.10039x^2 + 0.53559x. \end{aligned} \quad (8)$$

For strained Ge on relaxed  $\text{Si}_{1-x}\text{Ge}_x$ , the corresponding monotonic piecewise fit is

$$\begin{aligned} \Delta E_v^{\text{Ge/SiGe}}(x) &= 0.06302 + 2.45735u - 4.03457u^2 \\ &\quad + 2.34954u^3, \\ \Delta E_v^{\text{Ge/SiGe}}(x) &= 0.22907v + 0.43005v^2, \end{aligned} \quad (9)$$

Here the first line is used for  $0 \leq x \leq 0.8$  with  $u = 0.8 - x$ , and the second for  $0.8 \leq x \leq 1$  with  $v = 1 - x$ . All coefficients in Eqs. (8) and (9) are in eV; Eq. (9) reproduces the sampled Ge/ $\text{Si}_{1-x}\text{Ge}_x$  data with a maximum absolute deviation below 7 meV.

For the lineup-derived offsets in Fig. 4, the dominant uncertainty sources are (i) band-edge variability across alloy realizations and (ii) sensitivity to plateau selection for the lineup extraction. We therefore use a representative 0.04 eV offset uncertainty from two 25 meV band-edge terms, inferred as half of the 50 meV three-SQS gap spread in Fig. 2, and a 10 meV lineup term added in quadrature. The full numerical offset dataset, including per-composition realization counts, is provided in the supplementary material (Table S1).

Overall, we developed a unified first-principles workflow for band alignment in strained Si/ $\text{Si}_{1-x}\text{Ge}_x$  and Ge/ $\text{Si}_{1-x}\text{Ge}_x$  heterostructures across the full composition range. Combining SQS disorder modeling, potential-lineup extraction, a Mulliken-weight SOC valence correction, and hybrid-functional conduction edges, it yields smooth, internally consistent offsets with lineup uncertainty on the order of 10 meV and analytic expressions for continuum device simulation.

## ACKNOWLEDGMENTS

This work used Digital Research Alliance of Canada computational resources. The authors are grateful to David van Driel, Achilleas Bardakas, and L. Stehouwer for insightful discussions regarding experimental band gap values.

## DATA AVAILABILITY STATEMENT

Data, input files, and analysis scripts are available from the corresponding author upon reasonable request.

## AUTHOR DECLARATIONS

### Conflict of Interest

F. Beaudoin is the chief executive officer of Nanoacademic Technologies Inc. and owns equity in the company.

### Author Contributions

**N. M. Vegh:** Methodology; investigation; formal analysis; writing—original draft. **P. Philippopoulos:** Methodology; formal analysis. **R. J. Prentki:** Methodology; writing—review and editing. **W. Zhang:** Methodology. **Y. Zhu, F. Beaudoin, and H. Guo:** Supervision.

- <sup>1</sup>F. Schäffler, “High-mobility Si and Ge structures,” *Semicond. Sci. Technol.* **12**, 1515 (1997).
- <sup>2</sup>D. J. Paul, “Si/SiGe heterostructures: from material and physics to devices and circuits,” *Semicond. Sci. Technol.* **19**, R75 (2004).
- <sup>3</sup>L. Yang, J. R. Watling, R. C. W. Wilkins, M. Borić, J. R. Barker, A. Asenov, and S. Roy, “Si/SiGe heterostructure parameters for device simulations,” *Semicond. Sci. Technol.* **19**, 1174 (2004).
- <sup>4</sup>F. A. Zwanenburg, A. S. Dzurak, A. Morello, M. Y. Simmons, L. C. L. Hollenberg, G. Klimeck, S. Rogge, S. N. Coppersmith, and M. A. Eriksson, “Silicon quantum electronics,” *Rev. Mod. Phys.* **85**, 961 (2013).
- <sup>5</sup>L. M. K. Vandersypen, H. Bluhm, J. S. Clarke, A. S. Dzurak, R. Ishihara, A. Morello, D. J. Reilly, L. R. Schreiber, and M. Veldhorst, “Interfacing spin qubits in quantum dots and donors—hot, dense, and coherent,” *npj Quantum Inf.* **3**, 34 (2017).
- <sup>6</sup>G. Scappucci, C. Kloeffel, F. A. Zwanenburg, D. Loss, M. Myronov, J.-J. Zhang, S. De Franceschi, G. Katsaros, and M. Veldhorst, “The germanium quantum information route,” *Nat. Rev. Mater.* **6**, 926 (2021).
- <sup>7</sup>C. R. Anderson, “Efficient solution of the schrödinger–poisson equations in layered semiconductor devices,” *J. Comput. Phys.* **228**, 4745–4756 (2009).
- <sup>8</sup>F. Beaudoin, P. Philippopoulos, C. Zhou, I. Kriekouki, H. Guo, P. Galy, and M. Pioro-Ladrière, “Robust technology computer-aided design of gated quantum dots at cryogenic temperature,” *Appl. Phys. Lett.* **120**, 264001 (2022).
- <sup>9</sup>C. G. Van de Walle and R. M. Martin, “Theoretical study of band offsets at semiconductor interfaces,” *Phys. Rev. B* **35**, 8154 (1987).
- <sup>10</sup>R. G. Dandrea, C. B. Duke, and A. Zunger, “Interfacial atomic structure and band offsets at semiconductor heterojunctions,” *J. Vac. Sci. Technol. B* **10**, 1744 (1992).
- <sup>11</sup>C. G. Van de Walle, “SiGe heterojunctions and band offsets,” in *Properties of Silicon Germanium and SiGe: Carbon*, EMIS Datareviews Series No. 24 (INSPEC, London, 2000) pp. 149–157.
- <sup>12</sup>G. Di Liberto and G. Pacchioni, “Band offsets in semiconductor heterojunctions: concepts, methods, and modeling,” *J. Phys.: Condens. Matter* **33**, 415002 (2021).
- <sup>13</sup>R. L. Anderson, “Experiments on Ge-GaAs heterojunctions,” *Solid-State Electron.* **5**, 341–351 (1962).
- <sup>14</sup>M. M. Rieger and P. Vogl, “Electronic-band parameters in strained Si<sub>1-x</sub>Ge<sub>x</sub> alloys on Si<sub>1-y</sub>Ge<sub>y</sub> substrates,” *Phys. Rev. B* **48**, 14276 (1993).
- <sup>15</sup>L. Colombo, R. Resta, and S. Baroni, “Valence-band offsets at strained Si/Ge interfaces,” *Phys. Rev. B* **44**, 5572 (1991).
- <sup>16</sup>G. P. Schwartz, M. S. Hybertsen, J. Bevk, R. G. Nuzzo, J. P. Mannaerts, and G. J. Gualtieri, “Core-level photoemission measurements of valence-band offsets in highly strained heterojunctions: Si-Ge system,” *Phys. Rev. B* **39**, 1235 (1989).
- <sup>17</sup>H. Yaguchi, K. Tai, K. Takemasa, K. Onabe, R. Ito, and Y. Shiraki, “Characterization of Ge/SiGe strained-barrier quantum-well structures using photoreflectance spectroscopy,” *Phys. Rev. B* **49**, 7394 (1994).
- <sup>18</sup>M. Virgilio and G. Grosso, “Type-I alignment and direct fundamental gap in SiGe-based heterostructures,” *J. Phys.: Condens. Matter* **18**, 1021 (2006).
- <sup>19</sup>V. Michaud-Rioux, L. Zhang, and H. Guo, “RESCU: A real-space electronic structure method,” *J. Comput. Phys.* **307**, 593 (2016).
- <sup>20</sup>Nanoacademic Technologies Inc., “RESCU: Real-space electronic structure calculator,” <https://nanoacademic.com> (2026).
- <sup>21</sup>J. P. Perdew, K. Burke, and M. Ernzerhof, “Generalized gradient approximation made simple,” *Phys. Rev. Lett.* **77**, 3865 (1996).
- <sup>22</sup>A. Zunger, S.-H. Wei, L. G. Ferreira, and J. E. Bernard, “Special quasirandom structures,” *Phys. Rev. Lett.* **65**, 353 (1990).
- <sup>23</sup>H. J. Monkhorst and J. D. Pack, “Special points for brillouin-zone integrations,” *Phys. Rev. B* **13**, 5188 (1976).
- <sup>24</sup>A. Baldereschi, S. Baroni, and R. Resta, “Band offsets in lattice-matched heterojunctions: A model and first-principles calculations for GaAs/AlAs,” *Phys. Rev. Lett.* **61**, 734 (1988).
- <sup>25</sup>R. S. Mulliken, “Electronic population analysis on LCAO-MO molecular wave functions. I,” *J. Chem. Phys.* **23**, 1833 (1955).
- <sup>26</sup>J. Heyd, G. E. Scuseria, and M. Ernzerhof, “Hybrid functionals based on a screened Coulomb potential,” *J. Chem. Phys.* **118**, 8207 (2003).
- <sup>27</sup>J. Heyd, G. E. Scuseria, and M. Ernzerhof, “Erratum: “Hybrid functionals based on a screened Coulomb potential” [J. Chem. Phys. 118, 8207 (2003)],” *J. Chem. Phys.* **124**, 219906 (2006).
- <sup>28</sup>M. L. Yu, E. T. Croke, and T. C. McGill, “Measurement of the valence band offset in novel heterojunction systems: Si/Ge(100),” *J. Vac. Sci. Technol. B* **8**, 908–911 (1990).
- <sup>29</sup>Nanoacademic Technologies Inc., “QTCAD,” <https://nanoacademic.com/solutions/qtcad/> (2026).